

# Photoluminescence of Femtosecond Laser-irradiated Silicon Carbide

Y. Abdedou,<sup>1</sup> A. Fuchs,<sup>2</sup> P. Fuchs,<sup>2</sup> D. Herrmann,<sup>2</sup> S. Weber,<sup>3</sup> M. Schäfer,<sup>3</sup> J. L'huillier,<sup>3</sup> C. Becher,<sup>2</sup> and E. Neu<sup>1</sup>

<sup>1</sup>RPTU Koblenz, Erziehungswissenschaften 67663 Koblenz, Germany

<sup>2</sup>Saarländische Landesuniversität, 66123 Saarbrücken, Germany

<sup>3</sup>Institut für Schichtwachstum, Röntgen-Optimas, RPTU Koblenz, 67663 Koblenz, Germany

(\*Electronic mail: nruffing@rptu.de)

(Dated: 16 April 2024)

Silicon carbide (SiC) is the leading wide-bandgap semiconductor material, providing mature doping and device fabrication. Additionally, SiC hosts a multitude of optically active point defects (color centers), it is an excellent material for optical resonators due to its high refractive index and an outstanding material for mechanical resonators due to its high  $Q/f$  product. Moreover, epitaxial graphene layers can be grown as ultrathin electrodes and provide the potential to fine-tune color center resonances. These characteristics render SiC an ideal platform for experiments with single color centers towards quantum technologies including coupling color centers towards cooperative effects.

A crucial step towards harnessing the full potential of the SiC platform includes technologies to create color centers with defined localization and density, e.g. to facilitate their coupling to nano-photonic structures and to observe cooperative effects. Here, silicon vacancy centers ( $V_{Si}$ ) stand out as no impurity atom is needed and high-thermal budget annealing steps can be avoided. We characterize the effect of localized, femtosecond laser irradiation of SiC, investigating surface modifications and photoluminescence including Raman spectroscopy and optical lifetime measurements.

## I. INTRODUCTION

Silicon carbide (SiC) has seen tremendous improvements as a semiconductor platform in recent years. Together with these improvements it has also been established as a host material for single color centers and their applications in quantum technologies. Silicon vacancy centers ( $V_{Si}$ ) have several favorable characteristics to be employed in quantum technologies. In 4H-SiC, they exist in two different configurations<sup>1</sup> corresponding to a cubic and a hexagonal lattice site. The defects show zero phonon lines at 861 nm for  $V1$  (cubic) and 915 nm for  $V2$  (hexagonal) whereas the shorter wavelength falls into the detection window of standard silicon photodetectors. Moreover,  $V_{Si}$  do provide an optically readable ground-state spin with a zero field splitting of 4.5 MHz for  $V1$  and 70 MHz for  $V2$  which is straightforwardly addressable with standard RF components. However, the contrast of this optically detected magnetic resonance (ODMR) is comparably low (below 1%). An additional challenge is the fact that  $V_{Si}$  luminescence is hard to collect in (0001) SiC, because of the  $V_{Si}$  dipole orientation in the SiC lattice. (0001) material is however the material with the highest commercial availability. Milestones include super-radiance<sup>2</sup> from two color centers, near-transform limited emission even in photonic nanostructures<sup>3</sup> as well as magnetic sensors working under extremely harsh conditions like high pressure<sup>4</sup>.

Localized  $V_{Si}$  have been created by various techniques: ion implantation (focused ion beams<sup>5</sup> or implantation through a mask<sup>6</sup>) or laser writing<sup>7-9</sup>. Ion-based techniques in principle allow for the highest precision in localization which has been shown to be mainly limited by the straggle of the ions which is in the range of tens of nanometers for keV ion implantation<sup>10</sup>. However, they also create high levels of damage and potential additional defects. Laser writing has been investigated as an alternative that relies on highly non-linear processes. Previous

works suggest the involvement of 16 photons in the generation of a vacancy defect<sup>7</sup>. With such an extremely non-linear process, even an optical technology allows for precise localization that has been estimated to be as good as 80 nm<sup>7</sup>.

To address different applications in quantum technologies, not only controlling the spatial placement but also varying the density of color centers is crucial: whereas single photon sources naturally require using a single color center, higher density ensembles can be favorable for highly sensitive magnetic sensors based on optically-readable spins. In this case, higher defect density leads to brighter fluorescence and thus reduced photon shot noise in the read-out. Moreover, enhancing the density of defect ensembles may allow to observe the transition from uncoupled to collective emission (super-radiance)<sup>11</sup>.

Laser writing can be used to create single  $V_{Si}$  in 4H-SiC<sup>7</sup> as well as ensembles<sup>8,12</sup>. We here perform laser processing using a commercial laser structuring system. We elucidate if laser processing might be optimized using epitaxial graphene layers that can be used as transparent electrode to electrically tune color centers. We here report on the photoluminescence from localized laser irradiated areas, we analyze surface morphology, Raman spectra as well as photoluminescence spectra and lifetimes.

## II. SAMPLE PRE-TREATMENT

4-Inch (0001) oriented HPSI 4H-SiC Wafers purchased from Wolfspeed were diced into quadratic chips of  $< 10 \times 10$  mm<sup>2</sup>. Surfaces are chemically mechanically polished to a roughness of  $< 0.5$  nm according to manufacturer specifications. A first sample was solvent cleaned with acetone and isopropanol to remove the protective layer from dicing. It was then annealed in vacuum ( $5.5 \times 10^{-7}$  mbar) at 800°C for 3

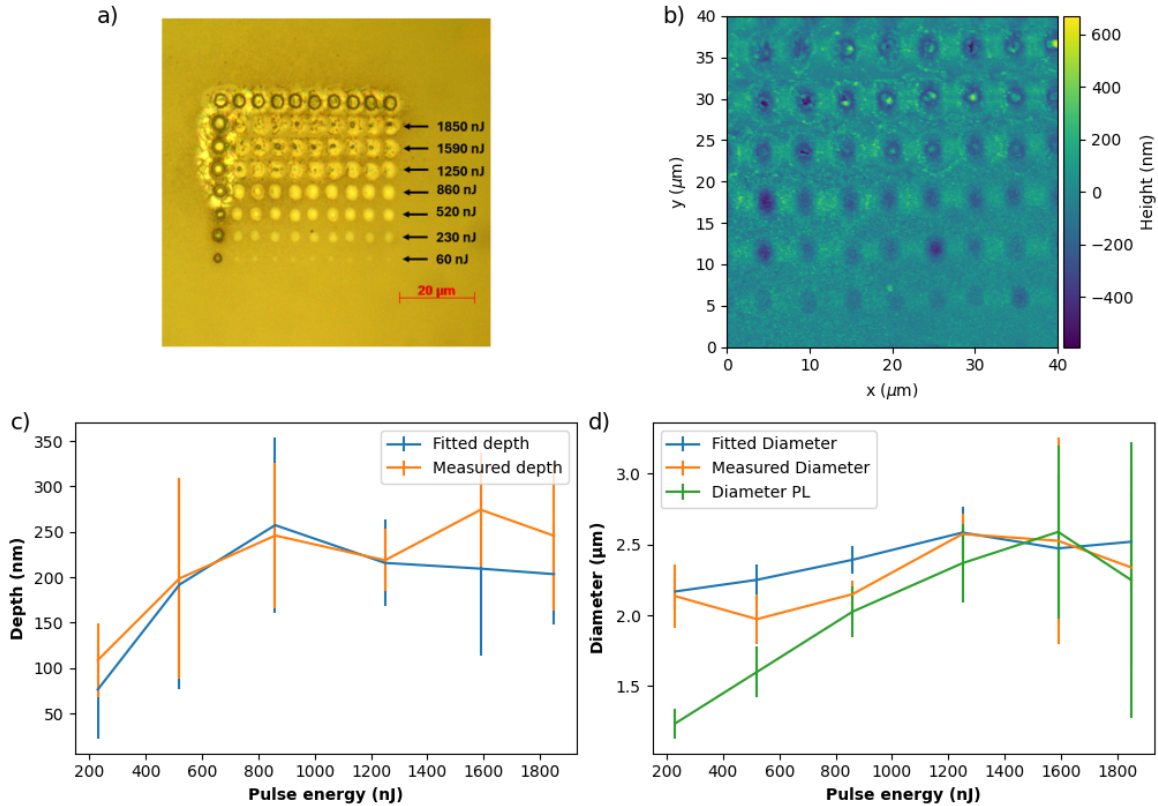


FIG. 1. **a)** White-light optical microscope image of the laser-processed pattern observed on the surface. The top row and the leftmost column serve as a marker, here we used a train of 5 pulses per spot at 1850 nJ for the top row, and 10 pulses per spot with pulse energy ranging from 60 to 1850 nJ for the leftmost column to induce a clear surface modification. The rows of spots visible within this marker angle have been processed using a single pulse of the laser with pulse energies ranging from 60 - 1850 nJ. **b)** AFM image of the laser written pattern. **c)** Average depth of the laser written spots in function of the laser pulse energy measured on spots profiles in orange and given by a fit with a Gaussian in blue. **d)** Average FWHM of the laser written spots in function of the laser pulse energy and size of the spots as determined from confocal PL maps.

hours. It has been observed that annealing at temperatures above  $600^{\circ}\text{C}$  reduces the initial  $V_{\text{Si}}$  concentration<sup>6,13</sup>) where ab-initio calculations show that  $V_{\text{Si}}$  migrate and recombine to form antisite-vacancy pairs ( $C_{\text{Si}}V_{\text{C}}$ )<sup>14,15</sup>. On the second sample, an epitaxial graphene layer was grown at  $1600^{\circ}\text{C}$ <sup>16</sup>.

### III. IRRADIATION OF PRISTINE HPSI SIC

We irradiate our SiC sample using an industrial-grade laser structuring system (BlueCut, Menlo Systems GmbH) with a wavelength of 1030 nm, a pulse duration of 383 fs and a repetition rate up to 1 MHz at a maximum pulse energy of 10  $\mu\text{J}$ . We focus the beam using a Thorlabs LMH-20X-1064 objective with 0.4 NA. The laser beam is linearly polarized. The focused beam had a calculated diameter of  $2.4 \mu\text{m}$  ( $1/e^2$ ). We obtain laser written patterns which we identify in our confocal laser-scanning fluorescence microscope (CLSM). FIG. 1 a) shows a white-light optical microscope image of the resulting pattern observed on the surface. The top row and the leftmost column serve as a marker, with a repetition rate of 10 kHz we used 5 pulses per spot at 1850 nJ, and 10 pulses per spot

with pulse energy ranging from 60 nJ to 1850 nJ for the leftmost column to induce a clear surface modification. The rows of spots visible within this marker angle have been processed using a single pulse of the laser with pulse energies ranging from (60 - 1850) nJ. The sample was then cleaned in acetone in an ultrasonic bath to remove particles occurring during the processing. This preliminary investigation by white-light microscopy already indicates a challenge in laser writing of (dense) color center ensembles: In the regions where multiple pulses have been used for processing, around the laser processed area a structure occurs that is due to laser ablation and re-deposition of material. This re-deposited material however will not be of high quality anymore, it is typically observed to be amorphous<sup>9</sup>.

To further analyze the structures induced on the surface especially at high pulse energies, we use atomic force microscopy (AFM) measurements carried out using a Park XE-70 AFM. The resulting image is shown in FIG. 1. b) and shows spots made with single pulses from 230 nJ to 1850 nJ. For the spots irradiated with 60 nJ, a surface modification is visible but we cannot extract its depth due to noise in our AFM. Figure 1 c) and d) summarize the depth and width

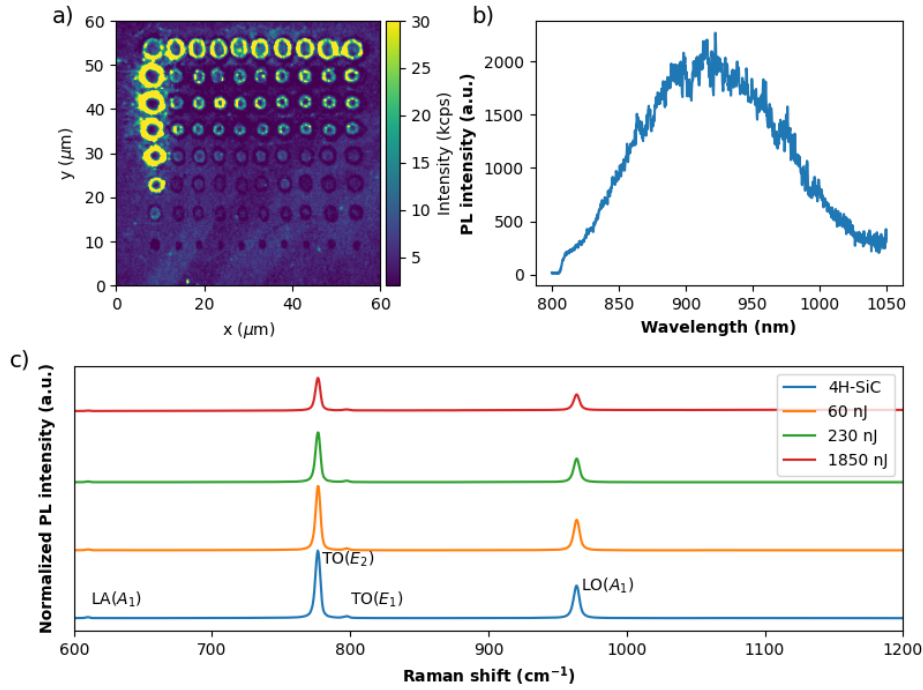


FIG. 2. **a)** Confocal PL map of the laser written pattern presented in FIG. 1 a). PL with wavelengths  $> 850$  nm was detected. From top to bottom, the rows have been written with 1850, 1590, 1250, 860, 520, 230 and 60 nJ (single pulse per spot) **b)** Exemplary PL spectrum from a spot irradiated with 860 nJ. **c)** Raman spectra of the unmodified pristine HPSI 4H-SiC and of spots made at different laser pulse energies of 60 nJ, 230 nJ and 1850 nJ. The spectra are offset vertically for clarity and have been recorded using a 532 nm laser.

of the surface structures. We add two datasets in each graph: we estimate the depth by measuring the distance between the surface and the deepest spot in the structure and we approximate the structure using a Gaussian fit. As discernible from Figure 1 c) and d) this gives us similar absolute values and a similar trend: size and width of the surface structures roughly grow with pulse energies up to 750 nJ. The diameter (width at  $1/e^2$ ) of the features obtained above 1250 nJ with roughly  $2.5 \mu\text{m}$  matches the diameter of the laser beam's Gaussian intensity profile that is  $2.4 \mu\text{m}$ . However, for pulse energies above 860 nJ, deviations from a Gaussian shape occur. We find a dimple with a hillock in the middle and ring shaped wall in the outer area. Due to the usage of a femtosecond laser, this is a typical mechanism when the ablation threshold is exceeded and the high energy of the pulse is able to break the covalent chemical bonds of SiC, ablating material<sup>17</sup>. In the context of localized creation of color centers, ablation processes have to be considered as a parasitic effect and will limit the creation of highly dense color center ensembles.

We use a home-built confocal laser-scanning fluorescence microscopes (CLSM) to investigate the photoluminescence (PL) of the laser written color centers. For room temperature characterization, we use continuous 785 nm laser light (Coherent OBIS LX 785) for excitation. In addition, we can couple a tunable, pulsed super-continuum laser source (NKT Super K-Extreme, typical pulse width  $< 100$  ps) which we use to measure the excited state lifetime  $\tau$  of the observed PL. In both cases, we use a 100x microscope objective with 0.9 NA (Zeiss EC EPN 100x/0,9 DIC) to focus the laser onto the sam-

ple and to collect the PL in a reflection geometry. We separate the PL and reflected laser light using a 785 nm edge dichroic mirror (Semrock Laser-Beamsplitter HC R785 lambda/5 PV flat). We detect the PL using silicon avalanche photo-diodes (APDS) for spectrally-integrated detection (Excelitas SPCM-AQRH-14). Alternatively, we sent the PL to a spectrometer equipped with a silicon CCD (Princeton Instruments Acton Standard SP-2558 Spectrometer with Pixis 256E CCD). In both cases, we use a 850 nm long pass filter for additional laser filtering.

Figure 2 a) shows a confocal PL map of the laser processed area. Localized PL is visible resembling the regular array that was processed by irradiating the SiC sample with single laser pulses. The bottom-most row has been exposed to 60 nJ laser pulses. Here, the PL intensity is even slightly reduced compared to the surrounding SiC. This could be attributed to local annealing that can be done with low pulse energy<sup>7</sup> and might reduce defects especially at the surface. We here compare our results to previously published results: Ref.<sup>7</sup> identifies the process that creates  $V_{Si}$  in SiC as highly non-linear. According to Ref.<sup>7</sup> 16 photons at a wavelength of 790 nm are involved in creating a single  $V_{Si}$  defect. For such a highly non-linear process (among other parameters), the peak intensity of the laser pulse will be crucial. We thus compare the peak intensity in our work to previous work. Ref.<sup>7</sup> reports a minimum pulse energy for creating single  $V_{Si}$  to be 10.7 nJ corresponding to  $22.2 \text{ TW/cm}^2$  (at 790 nm). In Ref.<sup>12</sup>, the laser pulse energy necessary to create defects with a 1030 nm femtosecond laser is found to be at 58 nJ. This corresponds to  $30.2 \text{ TW/cm}^2$  and

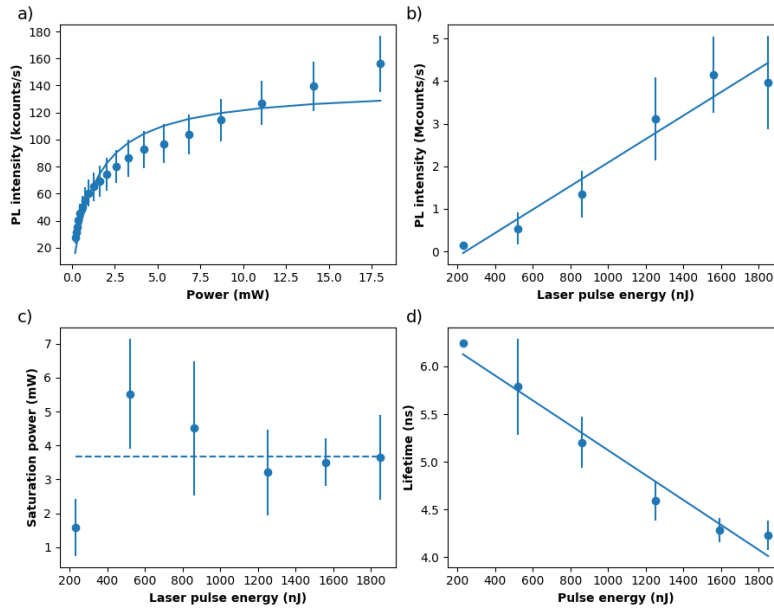


FIG. 3. **a)** Exemplary Saturation measurement recorded detecting PL with wavelengths longer than 850 nm generated with 230 nJ laser pulse. **b)** Saturation count rate detecting PL with wavelengths longer than 850 nm in function of laser pulse energy. **c)** Saturation power associated with the saturation count rate in function of the pulse energy, dashed line shows the mean saturation power at 4.72 mW. **d)** Lifetime measurements detecting PL with wavelengths longer than 850 nm in function of the pulse energy.

is thus slightly higher than in Ref.<sup>7</sup>. We also use 60 nJ as the lowest pulse energy. However, as we are using longer pulses and less tight focusing, in our case this only corresponds to 20.0 TW/cm<sup>2</sup>. We observe an onset of PL for the second lowest pulse energy we use which is 230 nJ corresponding to 76.6 TW/cm<sup>2</sup>. Thus, the onset of localized PL from laser irradiated areas is in accordance with previous work.

We then perform PL spectroscopy of the bright spots created by irradiation with single laser pulses. For all photoluminescent spots, we obtain typical spectra as displayed in Fig. 2b). This very broad PL spectrum without a discernible zero-phonon line has been identified as the typical PL signature of  $V_{Si}$  at room temperature<sup>18</sup>. The measured PL intensities and the fact that second order photon correlation measurements on the bright spots show no anti-bunching point to  $V_{Si}$  ensembles and are similar to previous work<sup>8</sup>.

In FIG. 1 c), we analyze the spatial dimension of the laser irradiated spots on our PL map. To this end, we fit the PL spots using a 2D Gaussian function to obtain their diameter ( $1/e^2$ ) and plot it in dependence of the laser pulse energy. We note that for higher pulse energies the shape of the luminescent spots deviates from Gaussian, however, the Gaussian fit is considered a good estimate to extract the diameter. PL spots grow in size up to a pulse energy of 1590 nJ, subsequently reaching a plateau. This finding is in accordance with our AFM measurements that show a similar trend. For comparison with AFM measurements, a linear estimation gives a growth rate of the PL spots with laser pulse energy of 1.00 nm/nJ (0.41 nm/nJ growth rate with AFM measurements).

We measure PL saturation curves for each laser irradiated spot and average over the measurements on the spots irradiated with the same pulse energy. Figure 3 a) exemplary shows

the saturation measurement for spots irradiated with 230 nJ. To correct the data for background, we perform a saturation measurement at a spot 10  $\mu$ m downward from the row written at 60 nJ. We correct the data points by subtracting the background. We note that the PL background also showed a saturation behavior. This might indicate that native point defects contribute to the background as reported previously<sup>12</sup>. Figure 3. b) shows the saturation count rate as a function of the writing pulse energy. Saturation count rates increase linearly with laser pulse energy indicating a linear increase of luminescent defects with pulse energy assuming a constant emission rate for each created defect. On the other hand, we will below discuss changes on excited state lifetimes that indicate non-radiative processes and thus changes in the emission rate per defect. the decreasing lifetimes pointing out to non-radiative decaying pathways for  $V_{Si}$  make it complicated to estimate the evolution on the number of  $V_{Si}$  with laser pulse energy. We also have to take into account the scattering of light in the highly damaged regions influencing the collected photoluminescence.

In addition modifying the surface profile (FIG. 1), increasing the pulse energy also changes the crystalline properties of SiC in the vicinity of the spots<sup>8,9,19</sup>. When aiming to create  $V_{Si}$ , due to their lower formation energy, carbon vacancies ( $V_C$ ) are also created nearby, which are not optically active. They provide non-radiative decay paths for  $V_{Si}$  therefore quenching their PL<sup>7,20,21</sup>. FIG.3. d) summarizes the lifetimes  $\tau$  extracted from PL measurements ( $> 850$  nm). Again, we obtain by averaging measurements from all spots irradiated with the same pulse energy. For spots irradiated with 230 nJ pulses, we find  $\tau = 6.2$  ns which matches  $\tau_{V_{Si}} = 6.1$  ns obtained for  $V_{Si}$  created using electron irradiation<sup>22</sup>.  $\tau$  linearly decreases with

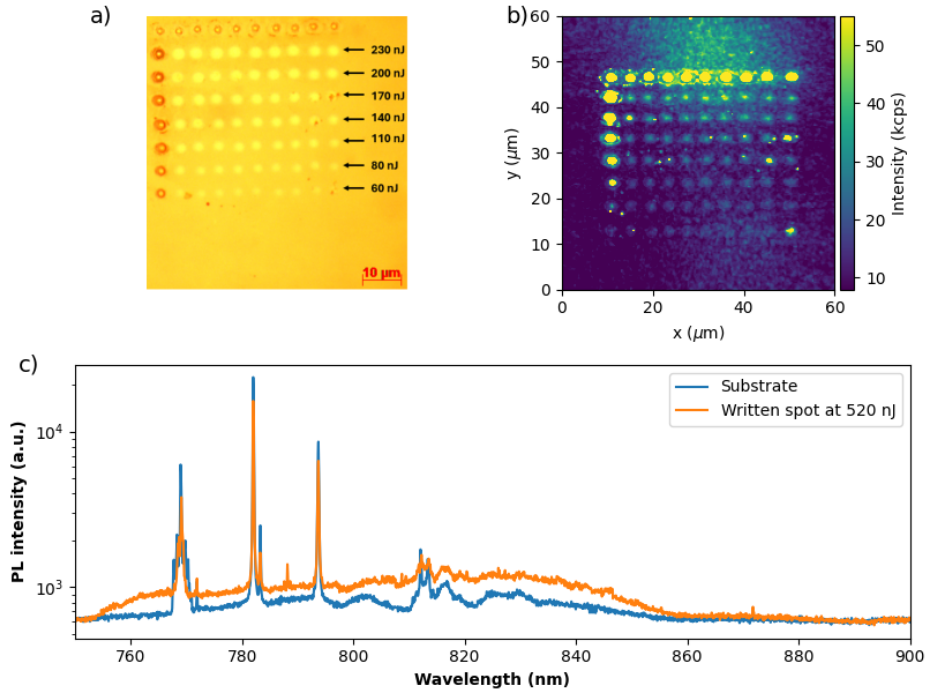


FIG. 4. **a)** White-light optical microscope image of the laser written pattern on the sample with graphene with higher pulse energy on the top row (230 nJ) and lower pulse energy on the bottom row (60 nJ) **b)** Associated confocal PL map of the laser written pattern. **c)** Low temperature spectra (4.3K) of the sample with graphene taken on an unprocessed area (blue) and a laser written spot (520 nJ) (orange).

pulse energy, indicating quenching by  $V_C$  and also potential interaction with extended defects due to laser irradiation. The decrease in  $\tau$  renders it challenging to estimate number of luminescent defects it might also indicate a change in the type of defect being created. We also have to take into account the scattering of light in highly damaged regions influences PL collection. In contrast, the saturation power as displayed in FIG.3 c) did not change with pulse energy.

FIG. 2. c) shows Raman spectra taken using a commercial Raman spectrometer using a 532 nm laser light on the pristine sample from an unprocessed area and from spots written at 60 nJ, 230 nJ and 1850 nJ. Compared to the reference Raman spectra from the unprocessed 4H-SiC, we observe on spectra taken from dimples made with single pulse at 60 nJ slight drop in peak intensities most notably on the  $TO(E_2)$  and  $LO(A_2)$  peaks. At 230 nJ and 1850 nJ, the decrease in peak intensities is even more significant being maximal for the 1850 nJ. While this Raman spectrum shows no sign of amorphous material even for 1850 nJ, the strong decrease in Raman peak intensity has been associated with significant crystal damage in previous work<sup>8</sup>.

#### IV. IRRADIATION OF HPSI WITH GRAPHENE LAYER

The second sample with an epitaxial graphene layer grown on top of a HPSI 4H-SiC substrate was processed using the same method described in the previous section, except using for this sample a repetition rate of 100 kHz. Figure 4 a) shows a white-light microscope image of a laser processed pattern,

having the same layout as presented in FIG. 1 a). In the single pulse region, we reduced the laser pulse energy to range from 60 nJ (bottom) to 230 nJ (top) or alternatively from 230 nJ to 520 nJ (pattern not shown). For this sample, we also created patterns for which we lifted the sample stage by 5  $\mu\text{m}$  or 10  $\mu\text{m}$  respectively, to move the laser focus into the bulk of our SiC sample. FIG. 4. b) shows a room temperature confocal PL map of the pattern from FIG. 4. a). The background PL is more pronounced compared to FIG. 2 a). Thus, the annealing and growth of the graphene layer did not aid in removing background PL in our case. We also note as a general finding that patterns deeper in the bulk show less PL than the patterns

To obtain more information on the defects created by the laser writing process, the sample with graphene was cooled down to 4.3K in a closed-cycle cryostat (CryoVac). In this cryogenic confocal setup, we excite PL using a tunable titanium sapphire laser (Sirah) operating at 737.19 nm focused on the sample with a microscope objective (Olympus MPLN 100x, NA = 0.9). PL light is collected using the same objective and reflected laser light is separated from the PL with a 740 nm dichroic mirror. Transmitted PL light is further filtered with a longpass filter and coupled to a single mode fiber that can either be connected to an APD (Excelitas SPCM-AQRH) or a spectrometer (Horiba iHR550) equipped with a 600 lines per mm grating and a Peltier cooled CCD camera.

We record various PL spectra at 4.3K. While our room temperature spectra as well as the lifetime measurements supported the localized creation of  $V_{Si}$ , we do not observe the ZPL emission of  $V_{Si}$  at cryogenic temperature and our findings do thus not confirm an efficient, localized creation of  $V_{Si}$ .

This finding is in accordance with<sup>12</sup>. Ref.<sup>12</sup>, reports  $V_{Si}$  in laser written spots but only a weak enhancement compared to their non-irradiated substrate. We note that potential  $V_{Si}$  in our substrate have been most probably eliminated due to the annealing in the graphene growth. Figure 4 c) compares cryogenic spectra recorded on SiC irradiated with a single 520 nJ pulse to non-irradiated SiC next to the pattern. Both spectra shows peaks associated to the TS center at 769 nm, 812 nm and 813 nm (TS1, TS2 and TS3<sup>23</sup>). To investigate differences between defect creation at the surface and in the bulk, we investigate the pattern created by lifting the sample 10  $\mu\text{m}$ . We find two distinct peaks when scanning the depth of the excitation laser focus (Figure 6 inset). We take spectra on one of the markers irradiated with multiple pulses as PL from spots irradiated with single pulses was too weak. Spectra taken in the depths corresponding to the two PL maxima reveal again the signature of the TS and additional broadband PL Figure 6. Raman lines in both spectra have similar intensity and width, hinting at similar levels of crystal damage. So we cannot conclude on any differences in defect creation when the laser focus is irradiating the SiC surface or the bulk. The TS defect is known to survive high annealing temperature, however, its microscopic origin remains unclear. We thus cannot use TS defects to learn more about the laser writing process. The absence of  $V_{Si}$  could indicate very high temperatures in the processed volume that anneal out  $V_{Si}$ . Additionally,  $V_{Si}$  have to be in their negatively-charged state to display the desired PL. So changes in the charge state due to the presence of other defects might also de-active  $V_{Si}$  PL.

For the sample with the graphene layer, we also observe a strong increase in saturation power observed at room temperature. Figure 5. a)-b) exemplary compare saturation measurements for the PL created by the 230 nJ and 520 nJ pulse. Saturation count rate in the pristine(graphene) sample were measured to be 139(204) kcounts/s and 351(259) kcounts/s, for 230 and 520 nJ respectively. Strikingly, the associated saturation powers are 1.38 mW and 5.21 mW in the pristine sample and 25.6 mW and 18.5 mW in the sample with graphene. Neither the strong increase in saturation power nor the loss in PL can be connected to the absorption of the graphene layer which is only 2.3%<sup>24</sup>.

We investigated the effect of epitaxial graphene on HPSI SiC on the creation of luminescent defects under femtosecond laser irradiation. In accordance with previous work, we do not observe efficient creation of  $V_{Si}$  centers, while spots with intense PL seem to be connected with strong surface structures (dimples) in a reference sample without graphene. Despite strong surface modification, we do not see signature of amorphous materials. To optimize the process, 4H-SiC with a more favorable crystal orientation and doping could be investigated as well as shorter laser wavelength and stronger focusing to enhance non-linear effects in comparison to sample heating.

<sup>1</sup>E. Sörman, N. T. Son, W. M. Chen, O. Kordina, C. Hallin, and E. Janzén, "Silicon vacancy related defect in 4H and 6H SiC," *Physical Review B* **61**, 2613–2620 (2000).

<sup>2</sup>D. M. Lukin, M. A. Guidry, J. Yang, M. Ghezellou, S. D. Mishra, H. Abe, T. Ohshima, J. Ul-Hassan, and J. Vučković, "Optical superradiance of a pair of color centers in an integrated silicon-carbide-on-insulator microres-

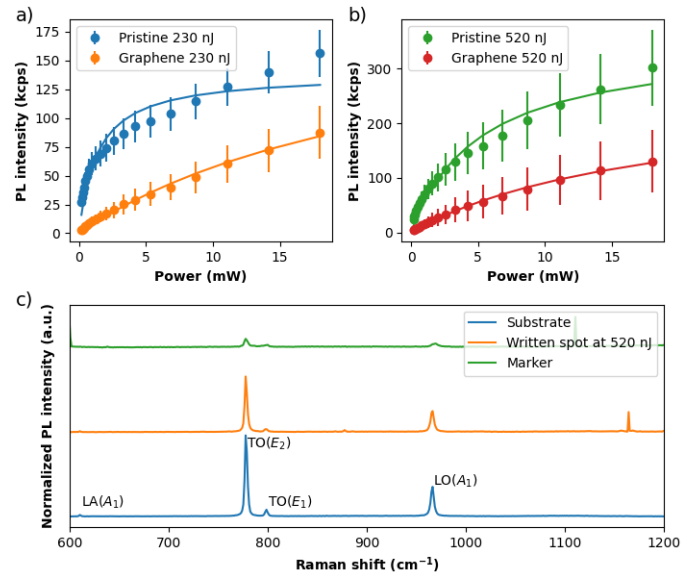


FIG. 5. a)-b) Comparison of saturation of PL induced via laser processing on the pristine 4H-SiC and 4H-SiC with a graphene layer. c) Raman spectra of the unprocessed HPSI 4H-SiC with graphene, a spot irradiated using a 520 nJ pulse and a marker. Spectra are offset vertically for clarity.

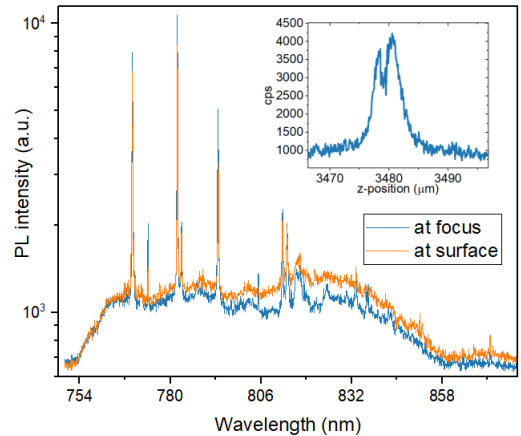


FIG. 6. PL spectra at 4.3K taken at different depth in the sample with graphene. The PL spectra are taking at spots corresponding to the two peaks in the inserted curve, with first peak on the left being on the surface and second peak being 2  $\mu\text{m}$  deep.

onator," (2022), 10.48550/ARXIV.2202.04845, publisher: [object Object] Version Number: 1.

<sup>3</sup>D. M. Lukin, M. A. Guidry, J. Yang, M. Ghezellou, S. Deb Mishra, H. Abe, T. Ohshima, J. Ul-Hassan, and J. Vučković, "Two-Emitter Multimode Cavity Quantum Electrodynamics in Thin-Film Silicon Carbide Photonics," *Physical Review X* **13**, 011005 (2023).

<sup>4</sup>J.-F. Wang, L. Liu, X.-D. Liu, Q. Li, J.-M. Cui, D.-F. Zhou, J.-Y. Zhou, Y. Wei, H.-A. Xu, W. Xu, W.-X. Lin, J.-W. Yan, Z.-X. He, Z.-H. Liu, Z.-H. Hao, H.-O. Li, W. Liu, J.-S. Xu, E. Gregoryanz, C.-F. Li, and G.-C. Guo, "Magnetic detection under high pressures using designed silicon vacancy centres in silicon carbide," *Nature Materials* **22**, 489–494 (2023).

<sup>5</sup>J. Wang, X. Zhang, Y. Zhou, K. Li, Z. Wang, P. Peddibhotla, F. Liu,

- S. Bauerdick, A. Rudzinski, Z. Liu, and W. Gao, "Scalable Fabrication of Single Silicon Vacancy Defect Arrays in Silicon Carbide Using Focused Ion Beam," *ACS Photonics* **4**, 1054–1059 (2017).
- <sup>6</sup>J.-F. Wang, Q. Li, F.-F. Yan, H. Liu, G.-P. Guo, W.-P. Zhang, X. Zhou, L.-P. Guo, Z.-H. Lin, J.-M. Cui, X.-Y. Xu, J.-S. Xu, C.-F. Li, and G.-C. Guo, "On-Demand Generation of Single Silicon Vacancy Defects in Silicon Carbide," *ACS Photonics* **6**, 1736–1743 (2019).
- <sup>7</sup>Y.-C. Chen, P. S. Salter, M. Niethammer, M. Widmann, F. Kaiser, R. Nagy, N. Morioka, C. Babin, J. Erlekampf, P. Berwian, and others, "Laser writing of scalable single color centers in silicon carbide," *Nano letters* **19**, 2377–2383 (2019), publisher: ACS Publications.
- <sup>8</sup>S. Castelletto, A. F. M. Almutairi, K. Kumagai, T. Katkus, Y. Hayasaki, B. C. Johnson, and S. Juodkazis, "Photoluminescence in hexagonal silicon carbide by direct femtosecond laser writing," *Optics Letters* **43**, 6077 (2018).
- <sup>9</sup>Z. Zhou, Z. Xu, Y. Song, C. Shi, K. Zhang, and B. Dong, "Silicon Vacancy Color Centers in 6H-SiC Fabricated by Femtosecond Laser Direct Writing," *Nanomanufacturing and Metrology* **6**, 7 (2023).
- <sup>10</sup>S. Pezzagna, D. Wildanger, P. Mazarov, A. D. Wieck, Y. Sarov, I. Rangelow, B. Naydenov, F. Jelezko, S. W. Hell, and J. Meijer, "Nanoscale Engineering and Optical Addressing of Single Spins in Diamond," *Small* **6**, 2117–2121 (2010), publisher: WILEY-VCH Verlag.
- <sup>11</sup>J. Gutsche, A. Zand, M. Büttel, and A. Widera, "Revealing superradiant emission in the single-to-bulk transition of quantum emitters in nanodiamond agglomerates," *New Journal of Physics* **24**, 053039 (2022).
- <sup>12</sup>S. Castelletto, J. Maksimovic, T. Katkus, T. Ohshima, B. C. Johnson, and S. Juodkazis, "Color Centers Enabled by Direct Femto-Second Laser Writing in Wide Bandgap Semiconductors," *Nanomaterials* **11**, 72 (2020).
- <sup>13</sup>M. Widmann, S.-Y. Lee, T. Rendler, N. T. Son, H. Fedder, S. Paik, L.-P. Yang, N. Zhao, S. Yang, I. Booker, and others, "Coherent control of single spins in silicon carbide at room temperature," *Nat. Mater.* **14**, 164–168 (2015), publisher: Nature Publishing Group.
- <sup>14</sup>M. Bockstedte, A. Mattausch, and O. Pankratov, "*Ab initio* study of the annealing of vacancies and interstitials in cubic SiC: Vacancy-interstitial recombination and aggregation of carbon interstitials," *Physical Review B* **69**, 235202 (2004).
- <sup>15</sup>X. Wang, M. Zhao, H. Bu, H. Zhang, X. He, and A. Wang, "Formation and annealing behaviors of qubit centers in 4H-SiC from first principles," *Journal of Applied Physics* **114**, 194305 (2013).
- <sup>16</sup>K. V. Emtsev, A. Bostwick, K. Horn, J. Jobst, G. L. Kellogg, L. Ley, J. L. McChesney, T. Ohta, S. A. Reshanov, J. Röhrl, E. Rotenberg, A. K. Schmid, D. Waldmann, H. B. Weber, and T. Seyller, "Towards wafer-size graphene layers by atmospheric pressure graphitization of silicon carbide," *Nature Materials* **8**, 203–207 (2009).
- <sup>17</sup>C. Wang, S. Kurokawa, T. Doi, J. Yuan, L. Fan, M. Mitsuhashi, H. Lu, W. Yao, Y. Zhang, and K. Zhang, "SEM, AFM and TEM Studies for Repeated Irradiation Effect of Femtosecond Laser on 4H-SiC Surface Morphology at Near Threshold Fluence," *ECS Journal of Solid State Science and Technology* **7**, P29–P34 (2018).
- <sup>18</sup>S. G. Carter, O. O. Soykal, P. Dev, S. E. Economou, and E. R. Glaser, "Spin coherence and echo modulation of the silicon vacancy in 4H-SiC at room temperature," *PHYSICAL REVIEW B* **92**, 161202(R) (2015).
- <sup>19</sup>J. Liu, Z. Xu, Y. Song, H. Wang, B. Dong, S. Li, J. Ren, Q. Li, M. Rommel, X. Gu, B. Liu, M. Hu, and F. Fang, "Confocal photoluminescence characterization of silicon-vacancy color centers in 4H-SiC fabricated by a femtosecond laser," *Nanotechnology and Precision Engineering* **3**, 218–228 (2020).
- <sup>20</sup>J. Steeds, G. Evans, L. Danks, S. Furkert, W. Voegeli, M. Ismail, and F. Carosella, "Transmission electron microscope radiation damage of 4H and 6H SiC studied by photoluminescence spectroscopy," *Diamond and Related Materials* **11**, 1923–1945 (2002).
- <sup>21</sup>H. Kraus, D. Simin, C. Kasper, Y. Suda, S. Kawabata, W. Kada, T. Honda, Y. Hijikata, T. Ohshima, V. Dyakonov, and others, "Three-dimensional proton beam writing of optically active coherent vacancy spins in silicon carbide," *Nano letters* **17**, 2865–2870 (2017), publisher: ACS Publications.
- <sup>22</sup>T. C. Hain, F. Fuchs, V. A. Soltamov, P. G. Baranov, G. V. Astakhov, T. Hertel, and V. Dyakonov, "Excitation and recombination dynamics of vacancy-related spin centers in silicon carbide," *J. Appl. Phys.* **115** (2014), <http://dx.doi.org/10.1063/1.4870456>.
- <sup>23</sup>M. Rühl, C. Ott, S. Götzinger, M. Krieger, and H. Weber, "Controlled generation of intrinsic near-infrared color centers in 4H-SiC via proton irradiation and annealing," *Applied Physics Letters* **113**, 122102 (2018), publisher: AIP Publishing LLC.
- <sup>24</sup>M. Rühl, L. Bergmann, M. Krieger, and H. B. Weber, "Stark tuning of the Silicon Vacancy in Silicon Carbide," *Nano Letters* **20**, 658 (2020), publisher: ACS Publications.

## ACKNOWLEDGMENTS

This work was funded by the Deutsche Forschungsgemeinschaft (DFG, German Research Foundation)– Project No. 429529648–TRR 306 QuCoLiMa ("Quantum Cooperativity of Light and Matter"). EN acknowledges support from the Quantum-Initiative Rhineland-Palatinate (QUIP). We thank Johannes Lehmeyer and Michael Krieger (FAU Erlangen, work-group H. Weber) for additional PL measurements of laser irradiated samples as well as the fabrication of the epitaxial graphene layer. We thank Stefan Dix (RPTU, work-group A. Widera) and Thomas Utz (RPTU, work-group G. von Freymann) for additional experiments on laser writing and Konstantin Gröpl (RPTU, work-group V. Schünemann) for his help with the Raman measurements.